Journal of Power Sources 196 (2011) 9445–9450

Contents lists available at ScienceDirect

Journal of Power Sources

journal homepage: www.elsevier.com/locate/jpowsour

Intermediate-temperature fuel cell employing thin-film solid acid/phosphate composite electrolyte fabricated by electrostatic spray deposition

Toshiaki Matsui[a,*], Toshimitsu Noto[a], Hiroki Muroyama[a], Masahiko Iijima[b], Koichi Eguchi[a]

[a] Department of Energy and Hydrocarbon Chemistry, Graduate School of Engineering, Kyoto University, Nishikyo-ku, Kyoto 615-8510, Japan
[b] TOYOTA Motor Corporation, Higashifuji Technical Center, Mishuku, Susono, Shizuoka 410-1193, Japan

ARTICLE INFO

Article history:
Received 21 May 2011
Received in revised form 25 June 2011
Accepted 3 July 2011
Available online 12 July 2011

Keywords:
Intermediate-temperature fuel cells
Composite electrolyte
Electrostatic spray deposition
Solid acid

ABSTRACT

An effective resistance of solid acid/phosphate composites was reduced by fabricating their thin-film electrolyte membranes for fuel cells operating at 100–300 °C. Solid acid and phosphate serve as an ionic conductor and supporting matrix, respectively, in these composites. Three-types of porous matrices were synthesized on a Pd film substrate by the electrostatic spray deposition technique, and then the solid acid was soaked under reduced pressure. The thin-film composite electrolytes showed almost the same conductivity in a wide temperature range of 100–200 °C, regardless of the difference in matrix microstructure. Above 200 °C, however, the microstructure of matrix significantly affected the thermal stability of the thin-film composite. The composite consisting of the matrix with the reticular structure, characterized by a three-dimensional interconnected porous network, achieved high thermal stability as well as low area specific resistance. Fuel cells employing thin-film membrane electrode assemblies were successfully operated at 200 °C, and the electrochemical measurements clarified the improvements.

1. Introduction

Fuel cells operating at the intermediate temperature range of 200–600 °C, so-called as intermediate-temperature fuel cells, are one of the attractive energy conversion devices alternative to combustion engines. However, the absence of appropriate ionic-conductors with high conductivity and stability in this temperature range has impeded the development of this system [1]. Recently, considerable efforts have been devoted to fabricate new ionic conductors operating especially at 100–300 °C [2–18]. A series of solid acids is the promising electrolytes among various kinds of candidates.

We have proposed new proton-conductive electrolytes based on solid acid/pyrophosphate composites, such as $AH_5(PO_4)_2/BP_2O_7$ (A = K, Rb, Cs and B = Si, Ti) [19–21]. In these composites, solid acid and pyrophosphate serve as an ionic conductor and supporting matrix, respectively. Note that the matrix species significantly affect the conductivity and the thermal behavior of composite electrolytes. For example, the combination of a SiP_2O_7 matrix was compared with a SiO_2 matrix for $CsH_5(PO_4)_2$ electrolyte [22,23]. The composite of $CsH_5(PO_4)_2/SiP_2O_7$ exhibited one order of magnitude higher conductivity than $CsH_5(PO_4)_2/SiO_2$, regardless of almost the same carrier concentration in the composites. This means that the interfacial interaction between the ionic conductor and the matrix is an important factor, which opens the new design concept for composite materials. Although the fuel cells employing these composite electrolytes were successfully demonstrated, the membrane electrode assembly (MEA) with the thickness of *ca.* 1 mm resulted in a large effective resistance [24]. Thus, the fabrication of thin-film electrolyte is imperative to overcome this issue for the practical application. However, the conventional synthesis route of pyrophosphate makes the thin-film fabrication difficult. In our previous studies, the matrix of SiP_2O_7 was synthesized by the chemical reaction of silica with an excess amount of phosphoric acid upon the several steps of heat-treatments [19]. The surface area of obtained pyrophosphate via this process was quite small, several square meters per gram, even with the usage of fumed silica. Therefore, the new technique is required to fabricate the thin-film matrix with porous network to provide the continuous path for ionic conduction.

Among the thin-film fabrication techniques, electrostatic spray deposition (ESD) offers many advantages; i.e., (i) simple set-up, (ii) ease in controlling the surface morphology, (iii) control of chemical composition, (iv) high deposition efficiency, and (v) inexpensive precursors [25–30]. This technique has been used to synthesize thin ceramic films of solid electrodes and electrolytes. Furthermore, the calcium phosphate coating has been tried for biomedical applications [28,29]. Thus, ESD is one of the feasible procedures for the fabrication of porous thin film consisting of binary components of silicon and phosphorus. In the ESD process, a precursor solution is electrostatically atomized by applying a high voltage, and then is ejected from a metal syringe nozzle towards a grounded

* Corresponding author. Tel.: +81 75 383 2523; fax: +81 75 383 2520.
E-mail address: matsui@elech.kuic.kyoto-u.ac.jp (T. Matsui).

0378-7753/$ – see front matter © 2011 Elsevier B.V. All rights reserved.
doi:10.1016/j.jpowsour.2011.07.004

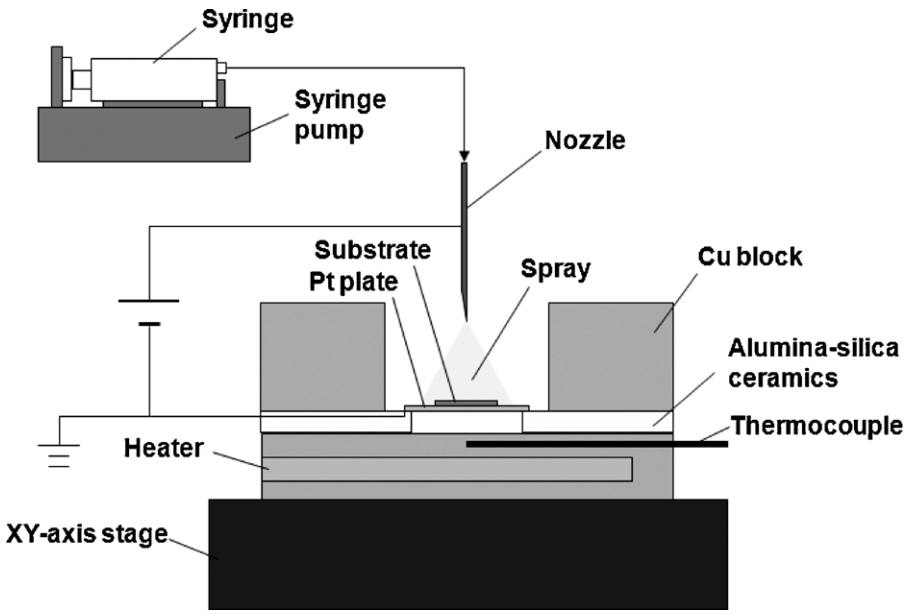

Fig. 1. Schematic illustration of the electrostatic spraying apparatus.

substrate. After the evaporation of solvent, a thin layer is formed on the substrate surface. Several physical and chemical deposition parameters affect the electrospray characteristics and coating morphology; i.e., deposition temperature and time, nozzle-to-substrate distance, applied voltage, the composition of precursor solutions, and the flow rate of precursor liquid. The morphology of film is also influenced by the subsequent heat treatment.

In this study, we aimed to reduce the effective resistance of solid acid/phosphate composite electrolyte by fabricating the thin-film membrane. ESD technique was applied to synthesize the phosphate matrix by optimizing the various parameters mentioned above, and three types of thin-film matrices with different morphology were synthesized. The influences of chemical composition and microstructure of matrices on the ionic conductivity and thermal stability were investigated. The performance of fuel cell with thin-film MEAs was also evaluated.

2. Experimental

2.1. Thin-film electrolyte

The schematic drawing of the ESD setup is shown in Fig. 1. The precursor solution was supplied to the nozzle by a syringe pump (Harvard apparatus, Model 11 plus). A high DC voltage power supply (Matsusada, HCZE) was used to generate a high potential difference between the nozzle and the grounded substrate. A stainless steel nozzle with a tilted outlet (apex angle 30°) was used (inner and outer diameter; 0.6 mm and 0.8 mm, respectively). The substrate temperature was controlled by the thermocouple set in the copper block. A precursor solution was prepared by dissolving H_3PO_4 (85 wt.%, Wako Pure Chemical Industries) and $(C_2H_5O)_4Si$ (Wako Pure Chemical Industries) in butyl carbitol (diethylene glycol monobutyl ether, $C_8H_{18}O_3$, Nacalai tesque). The molar concentration ratio between H_3PO_4 and $(C_2H_5O)_4Si$ was fixed to be 2.5:1.0. After deposition, the coatings were subjected to additional heat treatment in a furnace under reduced pressure. The pressure in the furnace was reduced by using the diaphragm pump (Tokyo Rikakikai Co., Ltd, DIVAC 0.6 L, arrival pressure; 800 Pa). Hereafter, the fabricated coatings were abbreviated as "Si–P–O matrix". Pd film with a thickness of 25 μm was used as a substrate and electrode (or anode) due to the high hydrogen permeability and electronic conductivity. Actually, the palladium substrate has been applied for the anode of intermediate-temperature fuel cell using ultrathin proton conductor of Y-doped $BaCeO_3$ [31]. In some cases, one face of Pd film was coated with the commercial 40 wt.% Pt/C powder (abbreviated as Pd film–Pt/C, Pt loading; 0.39 mg cm^{-2}, Johnson–Matthey) and then the thin-film matrix was fabricated on the Pt coated face.

After the fabrication of Si–P–O matrix, the molten proton conductor of cesium pentahydrogen diphosphate, $CsH_5(PO_4)_2$, was soaked at 160 °C under reduced pressure to form the composite electrolyte. The powder of $CsH_5(PO_4)_2$ was synthesized by drying an aqueous solution of Cs_2CO_3 (Aldrich) and H_3PO_4 (Wako Pure Chemical Industries, guaranteed reagent) with a molar ratio of 1:4 at 100 °C.

For ionic conductivity measurements and power generation tests, Pt/C carbon paper (BASF, Pt loading; 1.0 mg cm^{-2}, electrode area; 0.283 cm^2) was attached as an electrode (or cathode) to the other face of thin-film composite.

2.2. Pelletized electrolyte

The SiP_2O_7 matrix was prepared by the same procedure described in the literature [19]. The other matrix of $Si_3(PO_4)_4$ was prepared as follows. SiO_2 (Nihon Silica, AZ-200) and H_3PO_4 were mixed with a molar ratio of 1.0:1.3 in a crucible and heated at 200 °C for 3 h. The resulting sample was dried at 100 °C for 24 h, and then ground and heated at 122 °C for 24 h. The sample was finally subjected to the heat treatment at 400 °C for 6 h.

The composite electrolytes of $CsH_5(PO_4)_2/SiP_2O_7$ and $CsH_5(PO_4)_2/Si_3(PO_4)_4$ were prepared by mixing each powder in a molar ratio of 1:4 and 1:2, respectively. The volume ratios between solid acid and matrix in the former and latter composites were 33:67 vol.% and 28:72 vol.%, respectively. The membrane electrode assembly (MEA) was fabricated by uniaxial pressing of the composite powder with electrodes (13 mm diameter, *ca.* 1.3 mm thickness, and 0.283 cm^2 in electrode area). For ionic conductivity measurements, Pt/C carbon paper (BASF, Pt loading; 1.0 mg cm^{-2}) was used as electrodes. The anodic overpotential of four types of working electrodes were also evaluated at 200 °C by using the three-electrode cell with $CsH_5(PO_4)_2/SiP_2O_7$ composite electrolyte; (i) Pt/C carbon paper (BASF, Pt loading; 1.0 mg cm^{-2}),

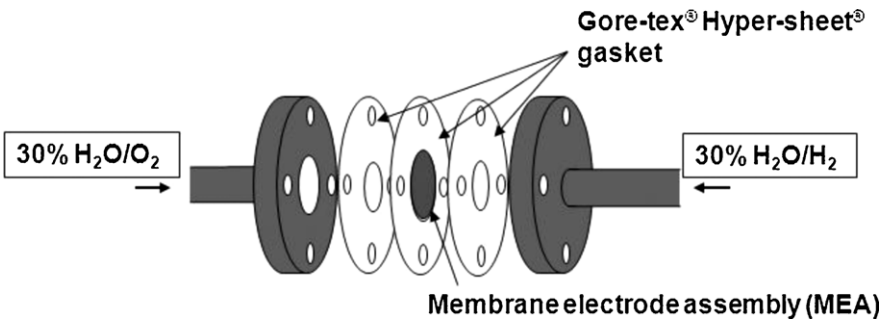

Fig. 2. Schematic illustration of cell configuration using thin-film MEA.

Table 1
ESD and calcination conditions of Si–P–O matrices.

Sample	Distance (nozzle to substrate) (mm)	Applied voltage (kV)	Liquid flow rate (ml h^{-1})	Deposition time (h)	Substrate temperature (°C)	Concentration of H_3PO_4 and $(C_2H_5O)_4Si$	Heat-treatment temperature (reduced pressure)
(a)	25	4.6	2.0	12	300	0.01 M and 0.004 M	200 °C for 3 h
(b)	25	4.6	2.0	12	300	0.04 M and 0.016 M	200 °C for 3 h
(c)	25	4.6	2.0	12	350	0.04 M and 0.016 M	200 °C for 3 h

(ii) Pd film with a thickness of 50 μm, (iii) Pd film–Pt/C (Pd film in 50-μm thick, Pt loading; 0.82 mg cm^{-2}), and (iv) Pd film–Pd/C (Pd film in 50-μm thick, Pd loading; 0.99 mg cm^{-2}). For the preparation of Pd film–Pt/C and Pd film–Pd/C, one face of Pd film was coated with 40 wt.% Pt/C (Johnson–Matthey) and 40 wt.% Pd/C powders, respectively. The Pd/C powder was prepared by the impregnation method. The carbon powder (V-XC72R, Cabot) was impregnated with the solution of $Pd(NO_2)_2(NH_3)_2$ (Tanaka Kikinzoku Kogyo). The mixture was kept on a steam bath at 80 °C to evaporate the solution, and then the resulting powder was calcined at 400 °C in a hydrogen atmosphere for 0.5 h. In this measurement, a reference electrode of Pt wire was attached on the electrolyte surface of the anode side, and Pt/C carbon paper (BASF, Pt loading; 1.0 mg cm^{-2}) was used as a counter electrode.

2.3. Characterization

The phase identification was conducted by X-ray diffraction with Cu Kα radiation (XRD, Rigaku, Ultima IV X-ray diffractometer). The typical working condition was 40 kV and 40 mA in air with a scanning speed of 2°/min. The surface and cross-sectional morphology of thin film were observed by scanning electron microscope (SEM, Shimadzu, SSX-550).

The electrochemical measurements were conducted by using the Solartron 1287 electrochemical interface and the Solartron 1260 frequency response analyzer. Proton conductivity was evaluated by ac impedance spectroscopy. The applied frequency was in the range of 0.1 Hz to 1 MHz with voltage amplitude of 10 mV. The measurements were carried out under 30% H_2O/Ar atmosphere,

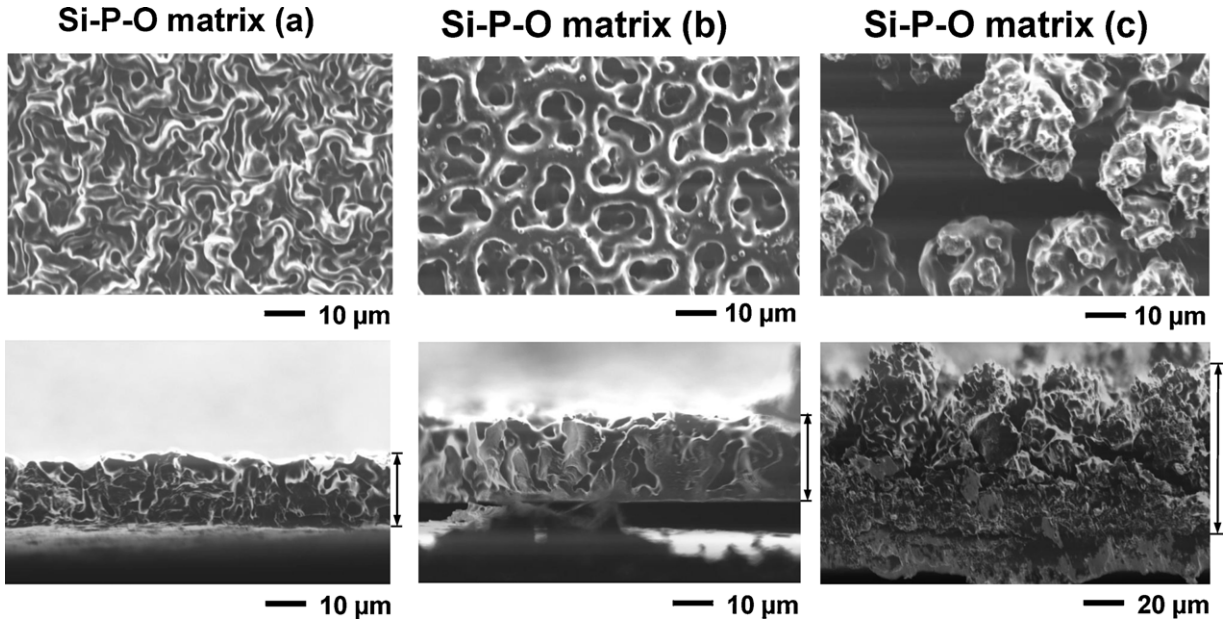

Fig. 3. SEM images of the surface and cross-sectional morphology for Si–P–O matrices (a)–(c) deposited on Pd substrate.

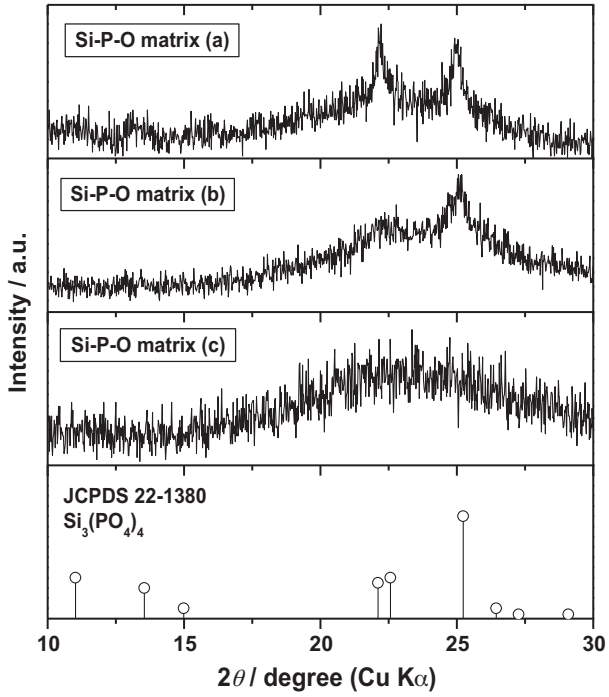

Fig. 4. XRD patterns of Si–P–O matrices (a)–(c) deposited on Pd substrate.

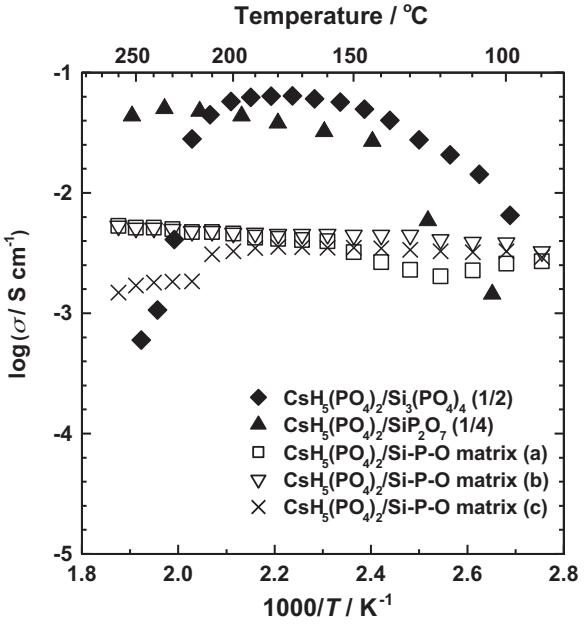

Fig. 5. Temperature dependence of the conductivity for $CsH_5(PO_4)_2/Si_3(PO_4)_4$ (molar ratio: 1/2), $CsH_5(PO_4)_2/SiP_2O_7$ (molar ratio: 1/4), and $CsH_5(PO_4)_2$/Si–P–O matrices (a)–(c) under 30% H_2O/Ar atmosphere.

which was prepared by bubbling dry Ar through water at 70 °C. At each temperature, samples were kept for 20 min to achieve the steady state. Fig. 2 shows the cell configuration used for power generation and polarization measurements. Humidified hydrogen and oxygen were fed to the anode (or working electrode) and cathode (or counter electrode), respectively. The water concentration in the feeding gas was controlled to be 30%, and the total flow of the gaseous mixture was fixed to be 50 ml min^{-1}.

3. Results and discussion

Three types of thin-film matrices were fabricated by controlling the various parameters for the ESD process. Fabrication conditions of matrices are summarized in Table 1; the substrate temperature and the concentration of the precursor solution were changed, and the other parameters were fixed. Surface and cross-sectional morphology of synthesized matrices are displayed in Fig. 3. The reticular structure was formed for Si–P–O matrices (a) and (b) with the pore sizes of several and 10 μm, respectively. This peculiar structure is characterized by a three-dimensional (3D) interconnected porous network. In contrast, porous films consisting of fractal agglomerates were deposited for Si–P–O matrix (c). Furthermore, the film growth rate appears to be related strongly with the microstructure because the film thickness of matrix (c) was quite large despite the same deposition time. Fig. 4 shows the XRD patterns of the three different matrices. The diffraction lines of Si–P–O matrices (a) and (b) were broad and ascribable to that of $Si_3(PO_4)_4$ [32], but those of Si–P–O matrix (c) appeared as a broad halo. Thus, the intended compound of SiP_2O_7 was not available in these conditions. This is because of the evaporation of phosphorus component during the deposition and heat-treatment processes prior to the crystalline growth. The low crystallinity of matrices will be related to the low heat-treatment temperature. Although the other parameters for the film fabrication process were controlled, a single phase of SiP_2O_7 matrix with the reticular structure was not formed. Therefore, the thin-film $Si_3(PO_4)_4$ matrix was applied in the following measurements, and the influence on electrochemical property was evaluated.

The temperature dependence of ionic conductivity for the thin-film electrolytes is shown in Fig. 5. For comparison, results of the pelletized composites of $CsH_5(PO_4)_2/Si_3(PO_4)_4$ and $CsH_5(PO_4)_2/SiP_2O_7$ are also depicted. The conductivity of $CsH_5(PO_4)_2/Si_3(PO_4)_4$ composite decreased drastically above 210 °C, while that of $CsH_5(PO_4)_2/SiP_2O_7$ was stable. In these two composites, the volume ratio between the ionic conductor of $CsH_5(PO_4)_2$ and matrix is almost the same (see Section 2). Therefore, the low chemical interaction between $CsH_5(PO_4)_2$ and $Si_3(PO_4)_4$ results in the low thermal stability, leading to the dehydration–condensation of $CsH_5(PO_4)_2$ component. This result also supports the importance of the chemical composition of matrix as described in the introduction part. The conductivity of thin-film electrolytes was one order of magnitude lower than that of the $CsH_5(PO_4)_2/Si_3(PO_4)_4$ composite at 150–200 °C. This tendency was caused by the small pore volume of the thin-film matrix, leading to the small amount of $CsH_5(PO_4)_2$ component per unit volume. Furthermore, the thin-film electrolytes showed almost the same conductivity in a wide temperature range of 100–200 °C, regardless of the difference in matrix structure. Such behavior is explained by the difference in the chemical interaction between $CsH_5(PO_4)_2$ and matrix. In the pelletized sample, the conductivity increases accompanying with the melt of $CsH_5(PO_4)_2$ at *ca.* 100–150 °C, whereas $CsH_5(PO_4)_2$ in the thin-film is kept in the molten state even at low temperatures. This will originate from the difference in the chemical state of matrix surface or the pore volume where $CsH_5(PO_4)_2$ component can infiltrate. Note that the conductivity of the composite with Si–P–O matrix (c) decreased above 200 °C as is the case of $CsH_5(PO_4)_2/Si_3(PO_4)_4$ in the pelletized form, though other thin-film composites maintained high conductivity up to 260 °C. This result indicates that the microstructure of the matrix significantly affects the thermal stability of the thin-film composite. Thus, the fabrication of matrix with the reticular structure provides the new design guide of composite electrolytes; the chemical interaction between an ionic conductor and matrix can be controlled by optimizing the matrix microstructure as well as the combination of

Table 2
Area specific resistance (ASR) of electrolytes at 200 °C.

Sample	Conductivity/ mS cm^{-1}	Thickness/cm	ASR/Ω cm^2
$CsH_5(PO_4)_2/SiP_2O_7$ (1/4)	44	0.12	2.7
$CsH_5(PO_4)_2/Si_3(PO_4)_4$ (1/2)	57	0.12	2.1
$CsH_5(PO_4)_2$/Si–P–O matrix (a)	4.6	0.0017	0.37
$CsH_5(PO_4)_2$/Si–P–O matrix (b)	4.6	0.0025	0.54
$CsH_5(PO_4)_2$/Si–P–O matrix (c)	3.3	0.0080	2.4

constituent materials. The area specific resistance of the composite electrolytes at 200 °C is listed in Table 2, which is an important factor for the development of fuel cell systems. The area specific resistance of thin-films (a) and (b) was quite lower than that of pelletized electrolytes. In this way, the reduction in effective resistance was accomplished by the ESD technique, but the obtained values were still higher than the target value of 0.2 Ω cm^2. Therefore, the further development of the matrix with an optimized 3D microstructure is required for the practical application.

In the previous study, we have reported that for the fuel cell composed of the CsH_2PO_4/SiP_2O_7-based composite electrolyte and Pt/C electrodes, the performance limitation was mainly due to the cathodic polarization at intermediate temperatures [24]. In this system, however, it is expected that the anode activity also affects the performance because the cell is supported by the dense substrate of Pd thin film. The hydrogen permeability of Pd and the roughness of the film substrate in contact with the composites are key factors, and the latter factor can be readily improved. The performance of four different anodes was evaluated by using the three-electrode cell with the pelletized $CsH_5(PO_4)_2/SiP_2O_7$ composite. The electrodes of Pd film–Pt/C and Pd film–Pd/C were fabricated to increase the roughness of substrate film by applying Pt/C and Pd/C powders on one face of Pd film, where was in contact with an electrolyte. The evaluated results are shown in Fig. 6, and the performance of anodes was in the following sequence:

Pt/C > Pd film–Pt/C > Pd film–Pd/C > Pd film

The Pt/C anode exhibited the lowest overpotential. The overpotential of Pd film was drastically reduced by the application of precious metal powders due to an increase in electrochemically active reaction sites. Furthermore, the overpotential of Pd film–Pt/C was lower

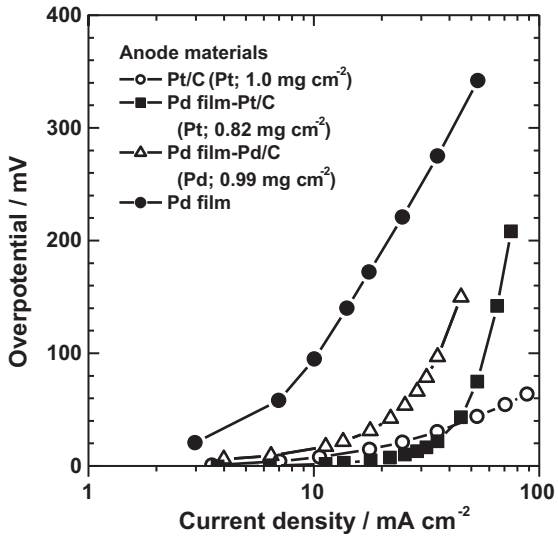

Fig. 6. Anodic overpotential of four different materials at 200 °C. Pelletized electrolyte, $CsH_5(PO_4)_2/SiP_2O_7$ composite; counter electrode, Pt/C; reference electrode, Pt wire; anode gas, 30% H_2O/H_2; cathode gas, 30% H_2O/O_2.

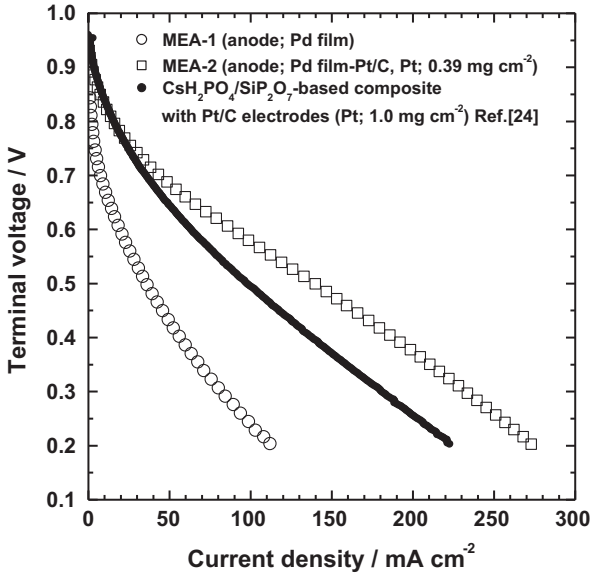

Fig. 7. *I–V* characteristics of MEA-1 and MEA-2 at 200 °C. Anode gas, 30% H_2O/H_2; cathode gas, 30% H_2O/O_2.

than that of Pd film–Pd/C. At this temperature range, Pt is more active for hydrogen oxidation as compared with Pd. Note that the performance of Pd film–Pt/C was comparable to that of Pt/C up to 50 mA cm^{-2}, while at high current density the overpotential of the former anode increased drastically. This will be caused by the limitation of hydrogen permeability rate through Pd film.

In the next step, the two-different MEAs with thin-film electrolytes were fabricated to evaluate the performance of fuel cells. Hereafter Pd film and Pd film–Pt/C were used as the substrates of the ESD process for MEA-1 and MEA-2, respectively. The thin-film composites were fabricated by the same procedure as that employed for Si–P–O matrix (b), and carbon paper with Pt/C was applied as a cathode.

MEA-1 : Pd film|$CsH_5(PO_4)_2$/Si–P–O matrix (b)|Pt/C

MEA-2 : Pd film–Pt/C|$CsH_5(PO_4)_2$/Si–P–O matrix (b)|Pt/C

Current–voltage characteristics of MEAs at 200 °C are shown in Fig. 7. The performance of the pelletized MEA, Pt/C|CsH_2PO_4/SiP_2O_7-based composite|Pt/C, is also depicted for comparison; in this composite electrolyte, the component of CsH_2PO_4 reacts with a part of SiP_2O_7 to form $CsH_5(PO_4)_2$ upon the heat treatment [24]. Corresponding impedance spectra at open circuit voltage are displayed in Fig. 8. The open circuit voltage was *ca.* 0.96 V regardless of MEAs, indicating that the gas-tight cells were successfully fabricated. The performance of MEA-2 was the highest among MEAs, but the significant improvement has not been achieved. In impedance spectra, the reduction in ohmic resistance can be confirmed for the thin-film MEAs as compared to the pelletized one. In MEA-1, however, the resistance in the high frequency region, ~10^3 Hz, was extremely higher than those in other MEAs. Furthermore, the characteristic frequency for the large semicircle in MEA-2 observed in Fig. 8(a) was about one order of magnitude lower than that in MEA-1 and comparable to that in the pelletized MEA. It has been clarified that high and low frequency processes in the two-electrodes system can be roughly assigned to anode and cathode reactions, respectively [24]. Therefore, obtained results support the low electrocatalytic activity of Pd film as discussed in Fig. 6. Although, in MEA-2, Pt/C catalyst layer located between the Pd film and composite electrolyte effectively enhanced the activity, the performance at

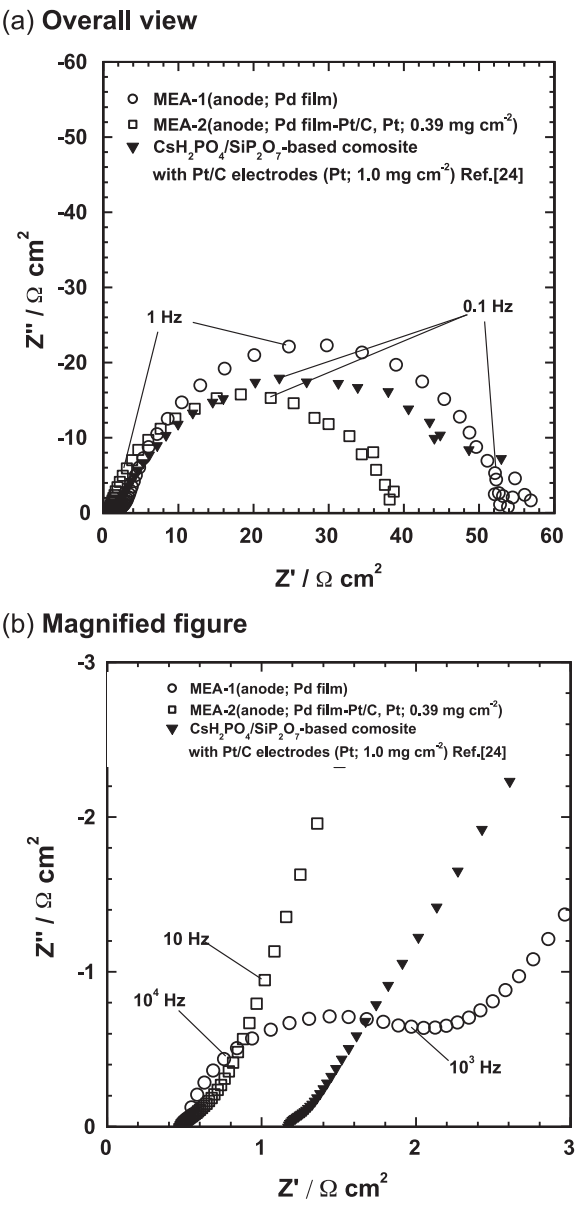

Fig. 8. Impedance spectra of thin-film MEA-1 and MEA-2 at open circuit voltage. (a) Overall view, (b) magnified figure; operating temperature, 200 °C; anode gas, 30% H_2O/H_2; cathode gas, 30% H_2O/O_2.

high current density was lower-than-expected. This behavior is also explained by the low hydrogen permeability of Pd film, but the application of porous substrate with current collecting capability will resolve this problem.

4. Conclusions

The porous matrices for the thin-film composite electrolytes were fabricated by the ESD method. Although the area specific resistance of thin-film electrolyte was successfully reduced, the obtained values were still higher than the target. The matrix microstructure significantly affected the thermal stability of the thin-film composite, and it was revealed that the matrix with the reticular structure was suitable for the intermediate-temperature application. These results indicated that the chemical interaction between ionic conductor and matrix can be controlled by optimizing the matrix microstructure as well as the combination of constituent materials. This will be the new design guide of composite electrolytes. The performance of MEA was enhanced by applying the modified Pd film substrate, but not to the expected level. Since this performance limitation was mainly due to the low hydrogen permeability of Pd substrate, further performance upgrade can be expected by applying the optimum substrate.

References

[1] T. Norby, Solid State Ionics 125 (1999) 1.
[2] S.M. Haile, D.A. Boysen, C.R.I. Chisholm, R.B. Merle, Nature 410 (2001) 910.
[3] D.A. Boysen, T. Uda, C.R.I. Chisholm, S.M. Haile, Science 303 (2004) 68.
[4] V.G. Ponomareva, N.F. Uvarov, G.V. Lavrova, E.F. Hairetdinov, Solid State Ionics 90 (1996) 161.
[5] V.G. Ponomareva, E.S. Shutova, Solid State Ionics 178 (2007) 729.
[6] J. Otomo, N. Minagawa, C.-J. Wen, K. Eguchi, H. Takahashi, Solid State Ionics 156 (2003) 357.
[7] H. Shigeoka, J. Otomo, C.-J. Wen, M. Ogura, H. Takahashi, J. Electrochem. Soc. 151 (2004) J76.
[8] H. Muroyama, T. Matsui, R. Kikuchi, K. Eguchi, J. Electrochem. Soc. 153 (2006) A1077.
[9] T. Matsui, S. Takeshita, Y. Iriyama, T. Abe, Z. Ogumi, J. Electrochem. Soc. 152 (2005) A167.
[10] T. Matsui, N. Kazusa, Y. Kato, Y. Iriyama, T. Abe, K. Kikuchi, Z. Ogumi, J. Power Sources 171 (2007) 483.
[11] M. Nagao, T. Kamiya, P. Heo, A. Tomita, T. Hibino, M. Sano, J. Electrochem. Soc. 153 (2006) A1604.
[12] Y. Daiko, A. Matsuda, J. JPN Petrol. Inst. 53 (2010) 24–32.
[13] T. Tezuka, K. Tadanaga, A. Hayashi, M. Tatsumisago, Solid State Ionics 177 (2006) 2463.
[14] K. Tadanaga, Y. Yamashita, A. Hayashi, M. Tatsumisago, Solid State Ionics 181 (2010) 187.
[15] X. Xu, S. Tao, J.T.S. Irvine, Solid State Ionics 180 (2009) 343.
[16] Y. Jin, K. Fujiwara, T. Hibino, Electrochem. Solid-State Lett. 13 (2010) B8.
[17] N.K. Becka, L.C.D. Jonghe, Electrochem. Solid-State Lett. 12 (2009) B11.
[18] M. Lia, K. Scott, Electrochem. Solid-State Lett. 12 (2009) B171.
[19] T. Matsui, T. Kukino, R. Kikuchi, K. Eguchi, Electrochem. Solid-State Lett. 8 (2005) A256.
[20] T. Matsui, T. Kukino, R. Kikuchi, K. Eguchi, J. Electrochem. Soc. 153 (2006) A339.
[21] H. Muroyama, K. Kudo, T. Matsui, R. Kikuchi, K. Eguchi, Solid State Ionics 178 (2007) 1512.
[22] T. Matsui, T. Kukino, R. Kikuchi, K. Eguchi, Electrochim. Acta 51 (2006) 3719.
[23] H. Muroyama, T. Matsui, R. Kikuchi, K. Eguchi, J. Phys. Chem. C 112 (2008) 15532.
[24] S. Yoshimi, T. Matsui, R. Kikuchi, K. Eguchi, J. Power Sources 179 (2008) 497.
[25] I. Taniguchi, R.C. van Landschoot, J. Schoonman, Solid State Ionics 156 (2003) 1.
[26] I. Taniguchi, R.C. van Landschoot, J. Schoonman, Solid State Ionics 160 (2003) 271.
[27] A. Princivalle, D. Perednis, R. Neagu, E. Djuradom, Chem. Mater. 16 (2004) 3733.
[28] S.C.G. Leeuwenburgh, J.G.C. Wolke, J. Schoonman, J.A. Jansen, Key Eng. Mater. 284–286 (2005) 199.
[29] S.C.G. Leeuwenburgh, M.C. Heine, J.G.C. Wolke, S.E. Pratsinis, J. Schoonman, J.A. Jansen, Thin Solid Films 503 (2006) 69.
[30] À. Varga, N.A. Brunelli, M.W. Louie, K.P. Giapis, S.M. Haile, J. Mater. Chem. 20 (2010) 6309.
[31] N. Ito, M. Iijima, K. Kimura, S. Iguchi, J. Power Sources 152 (2005) 200.
[32] JCPDS File card no. 22-1380, Joint Committee on Powder Diffraction Standards, Swarthmore, PA.